NJC

ROYAL SOCIETY OF CHEMISTRY

PAPER

View Article Online
View Journal | View Issue

Cite this: *New J. Chem.*, 2021, **45**, 12848

Tantalum(v) peroxido complexes as phosphatase inhibitors: a comparative study *vis-a-vis* peroxidovanadates†‡

Gangutri Saikia,* Hiya Talukdar, Kabirun Ahmed, Nand Kishore Gour and Nashreen S. Islam *

Received 28th February 2021,
Accepted 3rd June 2021

DOI: 10.1039/d1nj01005k

rsc.li/njc

The present work illustrates the synthesis and comprehensive characterization of novel peroxidotantalum(v) complexes anchored to water soluble polymer (WSP) matrices *viz.*, $[Ta_2(O_2)_6(carboxylate)_2]$–PA [PA = poly(sodium acrylate)] (**PATa**) and $[Ta(O_2)_3(sulfonate)_2]$–PSS [PSS = poly(sodium 4-styrene sulfonate)] (**PSSTa**) and their identification as potent inhibitors of acid phosphatase (ACP) activity. Using a set comprising tantalum(v) and vanadium(v) peroxides in similar macro ligand environments, and wheat thylakoid acid phosphatase as a model enzyme, it has been demonstrated for the first time that peroxidotantalum (pTa) derivatives are 2–3 fold more active as ACP inhibitors (IC_{50}: 0.34 μM for **PSSTa**) compared to their V containing analogues (IC_{50}: 1.22 μM). Enzyme kinetics analysis further revealed that the pTa and peroxidovanadate (pV) compounds tested, irrespective of the nature of their ligand environment, inhibit ACP function exclusively *via* a non-competitive pathway with K_i and K_{ii} values ranging between 0.2 and 4.7 μM. Importantly, under the effect of the enzyme catalase, the pTa compounds with a rate of peroxide loss as low as 0.92 μM min^{-1} (**PATa**) emerged to be remarkably more resistant to degradation relative to the corresponding pV compound, which degraded at a significantly faster rate (5.80 μM min^{-1}).

Introduction

Interest in the peroxido species of d^0 metal ions of group 5 seems to be never diminishing over the past decades.[1] Vanadium and its peroxido complexes in particular continue to have tremendous importance mainly owing to several significant discoveries relating to their biological and pharmacological role in the treatment of diabetes mellitus, malignancy and diseases caused by parasites.[1c,e–g,i] A few reports are also available on the biological activity of Nb compounds such as anticancer activity[2] and enzyme inhibitory activity.[3] On the other hand, the potential of peroxido compounds of tantalum, another group V element, as bioactive agents remains yet to be explored although tantalum and its compounds are not new in the field of medicinal chemistry. Being a bio-inert element with excellent biocompatibility and relatively non-toxic to animals, compounds of tantalum and its oxide based nanoparticles have been used as inert materials for implants[4] and various other therapeutic applications.[5,6] Recently, Starha *et al.* reported a new Schiff base–Ta complex, which exhibited strong cytotoxicity in cancer cells.[7] Notwithstanding these important findings, the contemporary interest in peroxidotantalum (pTa) compounds still mostly remains restricted to their utility as effective water soluble precursors to obtain Ta-based oxide materials for advanced technology applications.[1d] The aqueous chemistry of Ta is known to be limited to a very few available water soluble precursors.[1d,8]

It is pertinent to mention that our group has previously introduced a series of structurally defined and stable macrocomplexes by incorporating peroxide derivatives of d^0 metal ions *viz.*, V(v), Mo(vi), W(vi) and Nb(v) on water soluble polymers (WSPs) and explored their various bio-relevant aspects including their activity as inhibitors of enzyme phosphatases.[3c,9] Very recently, we have shown that peroxido compounds of V and Nb can effectively inhibit the activity of calcineurin, a serine/threonine phosphatase, *via* an uncompetitive pathway.[3c] The poly(acrylate) anchored pV species (**PAV**) also inhibited growth of lung carcinoma cells (A549)[10] in addition to displaying a vasomodulatory effect on rat aorta[11] and antibacterial[9a] properties. Importantly, the immobilized peroxidometallates

Department of Chemical Sciences, Tezpur University, Napaam, Tezpur 784028, Assam, India. E-mail: nsi@tezu.ernet.in, nashreen.islam@rediffmail.com; Fax: +91-3712-267006; Tel: +91-9435380222, +91-3712-267007

† This paper is dedicated to the memory of Professor T. Ramasarma. We shall remain ever grateful to late Professor T. Ramasarma, Department of Biochemistry, Indian Institute of Science, Bangalore, India for valuable suggestions and discussions.

‡ Electronic supplementary information (ESI) available: TGA data of **PATa** and **PSSTa**, experimental and theoretical IR spectral data of **PATa**, ^{13}C NMR spectral data of **PATa** for the stability study, L–B plots for inhibition of ACP activity in the presence or absence of (A) **DPV**, (B) **PAV** and (C) **PATa**. See DOI: 10.1039/d1nj01005k

synthesized by us exhibited enhanced stability as well as excellent ability to withstand decomposition to an appreciable extent in the presence of catalase, the ubiquitous reactive oxygen mopping enzyme present in nearly all living beings.[9b,d,e] This attribute is significant as the majority of the reported synthetic peroxidovanadium complexes have often suffered the hindrance of being hydrolytically unstable and toxic, which limits their clinical potential.[12] We anticipated that such limitations may be overcome by stabilizing the peroxidometallates by incorporating them into soluble macromolecular frameworks. Linear WSPs are essentially polychelatogens, which have been used extensively as supports in various fields of chemistry and biology, as these systems are usually free from negative attributes such as volatility, lability, toxicity and odor.[13]

Considering the significance of enzyme inhibition as an important pathway for action of inorganic drugs,[14] many vanadium derivatives including peroxidovanadates have been investigated as phosphatase inhibitors, as has been reviewed by Mclauchlan *et al.* recently.[15] Since phosphatases play a critical role in numerous signal transduction processes, this class of enzymes has become a key target for investigating metabolism, and for modifying cell signaling, and their selective inhibitors have prospective therapeutic roles.[15,16] Mechanistic insights into the biochemical potential of vanadium compounds have revealed that many of the reported compounds exert their action through mechanisms involving inhibition of enzymes, especially certain regulatory phosphatases.[1c,e,i,17] The insulin-mimetic activity of vanadium compounds has also been related to their inhibitory effect on phosphatases.[18] It has been observed that in most studies relative inhibitory potency *viz.* EC_{50} values of vanadium derivatives have been measured, while there are very few reports in the literature detailing the mechanism of such inhibition with defined K_i values.[15] It is worth highlighting that using enzyme kinetic analysis we have previously established for the first time that macromolecular peroxidovanadium complexes are highly potent classical non-competitive inhibitors of alkaline phosphatase (ALP) activity.[9b]

Continuing our research into exploration of the biochemical properties of peroxidometallates and taking into account the lack of information pertaining to the *in vivo* or *in vitro* effect of discrete pTa species on enzyme function, in the present study, our objective has been to undertake a comparative investigation of the activities of peroxido complexes of Ta and V with two different types of enzymes *viz.*, acid phosphatase and catalase. We have chosen wheat thylakoid membrane acid phosphatase since these enzymes are considered as effective models to study the metal induced inhibitory effect in membrane proteins.[19] Strategically, for the purpose of the present investigation, obtaining a set of water soluble and stable pV and pTa complexes in similar ligand environments has been the prerequisite.

Here, we present the synthesis and characterization of a pair of new peroxidotantalum complexes anchored to WSP matrices *viz.*, poly(sodium acrylate) (PA) and poly(sodium 4-styrene sulfonate) (PSS). We have previously gained access to pV compounds in a macroligand environment comprising PA and PSS polymers.[9a,b] We describe herein findings from our steady state kinetic study on the *in vitro* effect of polymer bound as well as free synthetic peroxido compounds of Ta(v) on the activity of ACP *vis-a-vis* their V(v) containing monomeric as well as polymer anchored analogues. Furthermore, we have investigated whether the pTa systems would exhibit resistance to degradation under catalase action as has been observed previously in the case of pV compounds.[9b] To date no previous study seems to exist pertaining to the interaction of pTa derivatives with catalase. Moreover, to our knowledge this is the first report to demonstrate that pTa systems can serve as effective inhibitors of phosphohydrolase enzymes.

Results and discussion

Synthesis and characterization

The inherent susceptibility of water soluble polymers with appropriate pendant functional groups to co-ordinate metal ions[20] provides a rather direct strategy for incorporation of low molecular weight metal complexes into macromolecular supports. The procedure adopted for the successful anchoring of the pTa moiety to the WSP chain to obtain the pTa complexes was based on the reaction of the precursor complex $Na_3[Ta(O_2)_4]\cdot H_2O$ with 30% H_2O_2 in the presence of the respective polymer in aqueous medium at ice-bath temperature, as demonstrated in Scheme 1. Maintenance of a pH of *ca.* 6 was found to be favourable for the desired synthesis in each case. Being essential polyelectrolytes, the degree of dissociation as well as type and extent of co-ordination of the water soluble polymers used in the present study, are known to be pH dependent.[21]

An additional pivotal component of the strategy is the maintenance of the required time and temperature for the successful formation of the complexes. The final product was obtained from the homogeneous reaction mixture by inducing precipitation with the addition of acetone. The microcrystalline products obtained were kept for several days *in vacuo* at temperature < 30 °C without any significant loss of activity.

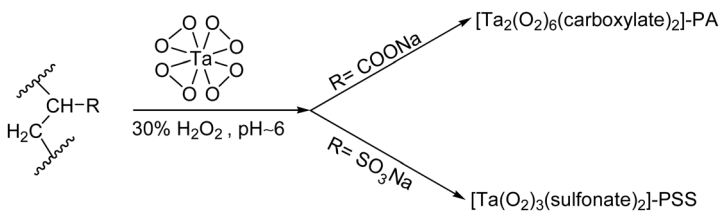

Scheme 1 Soluble polymer anchored pTa complexes. "∿∿" represents the polymer chain.

The newly synthesized macrocomplexes were characterized by analytical as well as spectroscopic techniques including FT-IR, Raman, ^{13}C NMR and also thermogravimetric analysis, which confirmed the formation of the complexes. The elemental analysis data revealed the presence of three peroxido groups per metal centre in the case of both the **PATa** and **PSSTa** complexes. The tantalum loading on the polymer matrix, determined on the basis of the metal percentage obtained from EDX along with inductively coupled plasma optical emission spectrophotometric (ICP-OES) analysis, was observed to be 1.62 and 0.85 mmol g^{-1} for compounds **PATa** and **PSSTa**, respectively. The diamagnetic nature of the peroxidotantalum complexes was evident from the magnetic susceptibility measurement, which indicated the presence of metal centres (Ta) in their +5 oxidation states.

SEM and energy dispersive X-ray analysis

The morphological changes occurring on the surface of the polymeric support after metal complex incorporation have been studied by scanning electron microscopy (SEM). The SEM images of supported metal complexes **PATa** and **PSSTa** showed significant roughening of their surfaces compared to the smooth surface of the respective virgin polymer, indicating that the metal complexes are distributed across the polymeric surface as seen in Fig. 1.

The energy dispersive X-ray analysis data clearly revealed the presence of Ta in addition to C, O, and Na as constituents of compounds **PATa** and **PSSTa** [Fig. 1(e) and (f)]. The existence of S in compound **PSSTa** was confirmed from its EDX spectrum [Fig. 1(f)]. The composition of the compounds derived from EDX analysis data agreed well with the results obtained from elemental analysis.

IR, Raman and electronic spectral analysis

The IR and Raman spectra of the complexes are presented in Fig. 2 and 3. Characteristic differences were observed in the spectral pattern of the metal incorporated polymer complexes compared to the pure polymer, indicating successful anchoring of the peroxidometallate species on the polymer matrix.

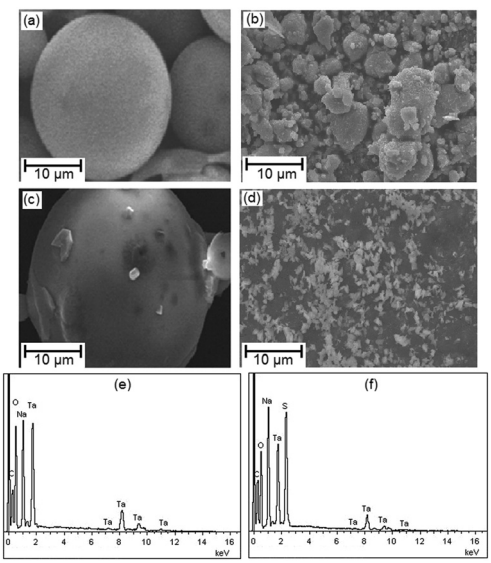

Fig. 1 Scanning electron micrographs of (a) PA, (b) **PATa**, (c) PSS, and (d) **PSSTa**. EDX spectra of (e) **PATa** and (f) **PSSTa**.

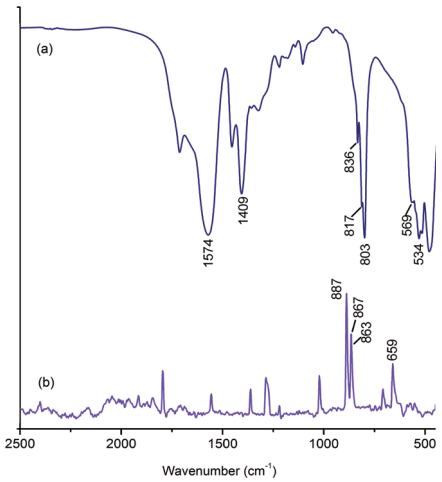

Fig. 2 (a) IR and (b) Raman spectra of **PATa** (recorded in the solid state).

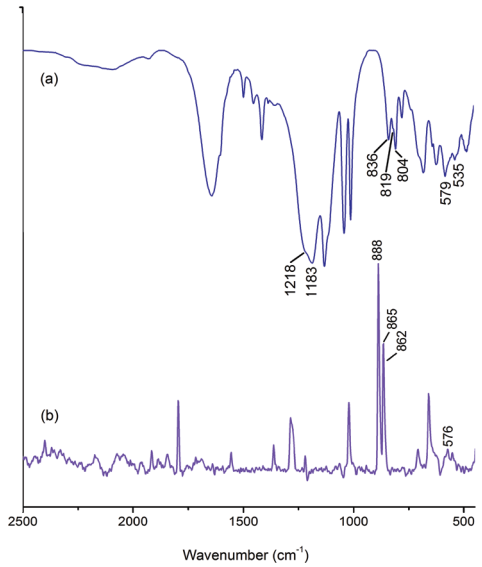

Fig. 3 (a) IR and (b) Raman spectra of **PSSTa** (recorded in the solid state).

Three absorptions corresponding to ν(O–O) vibrations were observed in the 800–840 cm^{-1} region depicting the presence of three peroxido groups per metal centre in the case of both **PATa** and **PSSTa**.[1d,22] In addition to this, ν_{as}(Ta–O_2) and ν_s(Ta–O_2) absorptions were detected in the 500–600 cm^{-1} range.[1d,22] The Raman spectra of the complexes complimented the IR results by displaying bands for ν(O–O), ν_{as}(Ta–O_2) and ν_s(Ta–O_2) in the respective region as shown in Table 1.

The available literature pertaining to metal–carboxylate coordination shows that the $\Delta\nu = \nu_{as}(COO) - \nu_s(COO)$ relationship has been derived as an important criterion to determine the mode of carboxylate binding to a metal centre,[9b,23] and it is also applicable to polycarboxylates as well as poly(acrylates).[9b,24] The IR spectrum of complex **PATa** displayed typical bands for the

Table 1 IR and Raman spectral data for compounds **PATa** and **PSSTa**

Assignment		**PATa** (cm^{-1})	**PSSTa** (cm^{-1})
ν(O–O)	IR	836(sh), 817(sh), 803(s)	836(m), 819(sh), 804(m)
	R	887(s), 867(s), 863(sh)	888(s), 865(s), 862(sh)
ν_{as}(M–O_2)	IR	569(sh)	579(m)
	R	659(m)	576(vw)
ν_s(M–O_2)	IR	534(s)	535(sh)
	R	441(s)	437(s)
ν_{as}(COO)	IR	1574(s)	
	R	1554(m)	
ν_s(COO)	IR	1409(m)	
	R	1368(m)	
ν_{as}(S–O)	IR		1218(sh), 1183(s)
	R		1283(m), 1221(vw)

s, strong; m, medium; vw, very weak; sh, shoulder.

ν_{as}(COO) and ν_s(COO) modes at 1574 cm^{-1} and 1409 cm^{-1}, respectively, as shown in Fig. 2(a), while those of free PA were observed at 1565 cm^{-1} and 1409 cm^{-1}. The $\Delta\nu$ (165 cm^{-1}) value obtained from the spectrum of **PATa** is close to that observed for free PA ($\Delta\nu$ = 157 cm^{-1}), which suggests a bridging bidentate mode of co-ordination of the carboxylate group.[9b,23,24c] An additional IR band observed in the region of 1713 cm^{-1} indicated the existence of free carboxylic acid groups in the complex.[9b] Three typical absorptions for ν(O–O) stretching vibrations were seen at 836, 817, and 803 cm^{-1}, suggesting the formation of triperoxidotantalum species in complex **PATa** along with bands at 534 and 551 cm^{-1} for ν_s(Ta–O_2) and ν_{as}(Ta–O_2) vibrations, respectively.[1d,22] Well resolved Raman bands appeared at 887, 867, and 863 cm^{-1} for ν(O–O) stretching in addition to the ν_s(Ta–O_2) band at 441 cm^{-1} and ν_{as}(Ta–O_2) band at 659 cm^{-1}.

The IR spectrum of the pure polymer PSS has shown bands at 1197 and 1039 cm^{-1} representing ν_{as} and ν_s(S–O) stretching modes of the pendant sulfonate group.[9b,25] After complexation, in addition to the symmetric stretching band at 1038 cm^{-1}, a distinct splitting pattern was observed at 1218 and 1183 cm^{-1} in the spectrum of **PSSTa**, which may be attributed to the complexed sulfonate group.[9b] The appearance of the vibration at 1218 cm^{-1} in the complex denoted the existence of free sulfonate groups.[9b] The characteristic absorptions of the phenyl group and CH_2 bending were exhibited at 1639 and 1496 cm^{-1}, respectively. The absorption peaks for the ν(O–O) stretching vibration appeared at 804, 819 and 836 cm^{-1}. The medium intensity bands at 579 and 535 cm^{-1} have been assigned to ν_{as}(Ta–O_2) and ν_s(Ta–O_2) vibrations, accordingly. The Raman spectrum of the complex displayed bands at 888, 865 and 862 cm^{-1} for ν(O–O) stretching. The metal oxygen symmetric and antisymmetric vibrations were seen at 437 and 576 cm^{-1}, respectively.

The presence of lattice water in the complexes has been confirmed by the appearance of a strong and broad absorption band at 3400–3500 cm^{-1} which has been ascribed to ν(OH) stretching.

The electronic spectra of macrocomplexes **PATa** and **PSSTa** displayed a broad band in the region 220–300 nm which has been ascribed to tantalum-peroxido species (Ta(η^2-O_2)) on the basis of available literature reports.[26]

^{13}C NMR studies

^{13}C NMR spectral analysis plays a decisive role in determining the mode of co-ordination of the macromolecular ligands to the metal centres. The ^{13}C NMR data of the polymer bound metal complexes and that of the pure polymers are presented in Table 2.

The spectrum of pure poly(sodium acrylate) showed, apart from the signals due to the –CH_2 and –CH groups of the polymer chain, peaks due to C atoms of carboxylate groups centred at 184 and 183 ppm [Fig. 4(a)].[13b,27] The two closely spaced peaks observed in this region are likely to be due to the presence of carboxylate as well as –COOH groups of the polymer in solution. The spectrum of polymeric complex **PATa** displayed an additional peak at 215 ppm attributable to the complexed carboxylate group.[3b,c,9b] A downfield shift of $\Delta\delta$ ($\delta_{complex} - \delta_{free\ carboxylate}$) $\approx$ 31 ppm of the compound was observed, which is in accord with the previously obtained values for other polyacrylate incorporated peroxidometal compounds bonded in a bidentate fashion.[3b,c,9b] This suggested the successful anchoring of the monomeric metal complexes on poly(sodium acrylate) through the pendant carboxylate group.

The ^{13}C NMR spectal pattern of the **PSSTa** complex shown in Fig. 5(b) remained practically unchanged after complexation *vis-a-vis* the virgin polymer spectrum. Since the Ta(v) centres are linked to the polymer through the pendant sulfonate groups, which are well separated from the chain and ring carbon atoms of the polymer matrix, the above observation is not unexpected.

TG-DTG analysis

The TG-DTG plots along with the thermogravimetric analysis data of polymer bound compounds **PATa** and **PSSTa** are presented in Fig. 6 and 7, and Table S1 (ESI‡), respectively. The compounds underwent multistage degradation upon heating up to 700 °C. It is noteworthy that, unlike many reported peroxidometal compounds,[1d,28] the immobilized pTa complexes

Table 2 ^{13}C NMR chemical shifts for polymer anchored pTa compounds **PATa** and **PSSTa**

Chemical shift (ppm)										
	Carboxylate carbon				Ring carbon					
Compound	Free	Complexed	CH	CH_2	C1	C2	C3	C4	C5	C6
PA	184.50		45.52	36.10						
PATa	184.91	215.54	45.90	36.11						
PSS	—	—	40.52	44.14	140.35	128.84	125.57	148.55	125.35	128.17
PSSTa	—	—	40.81	43.58	140.37	128.20	125.56	148.87	125.33	128.17

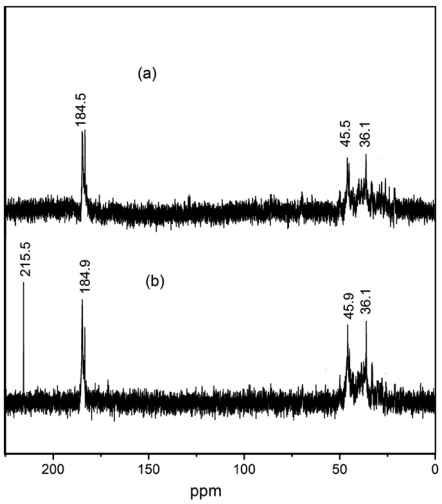

Fig. 4 ^{13}C NMR spectra of (a) PA and (b) **PATa** in D_2O (70 g L^{-1}) at pH ≈ 8.

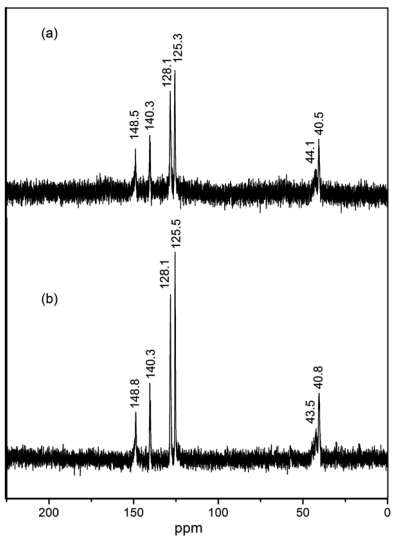

Fig. 5 ^{13}C NMR spectra of (a) PSS and (b) **PSSTa** in D_2O (70 g L^{-1}) at pH ≈ 8.

did not explode on heating. The first stage of degradation due to the release of water of crystallization occurs between room temperature and *ca.* 110 °C for both complexes. This was followed by the decomposition of peroxido groups in the subsequent step. Complete loss of peroxido groups from the compounds was confirmed from the absence of a peroxido band in the IR spectra of the degraded product isolated at this stage. Heating of complex **PATa** after the initial loss of peroxido groups leads to its further decomposition in the temperature range of 329–605 °C, which may be attributed to the decarboxylation and breakage of the polymer chain.[9b] The TG-DTG profile of **PATa** agreed well with the previously reported thermogravimetric analysis of other polyacrylate anchored peroxidometal compounds.[3c,9] The residue after complete degradation of **PATa** was found to be 54.7%. FT-IR spectral analysis of the residual mass was carried out, which

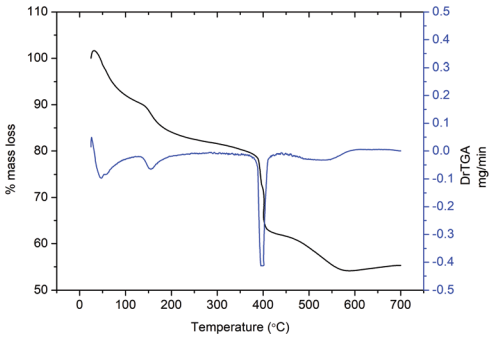

Fig. 6 TG-DTG plot of **PATa**.

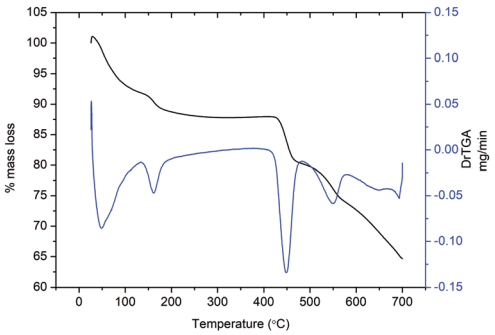

Fig. 7 TG-DTG plot of **PSSTa**.

showed bands at 867 cm^{-1} and 611 cm^{-1}, suggesting the existence of tantalum oxido groups in the residual moiety.[29]

Along with that, an additional band at 1443 cm^{-1} was observed which may be ascribed to sodium carbonate species present in the residue along with oxidotantalate.[3c] It has been reported earlier that thermal decomposition of sodium acrylate produces sodium carbonate in addition to CO_2 and CO as final decomposition products.[30]

In the case of **PSSTa**, two stages of degradation were observed in the temperature range of 400–697 °C after the initial dehydration step and the complete loss of peroxido groups. This may be ascribed to the loss of sulfonate groups as well as the rupture of the polymer chain with the release of ethylene, water, SO_2 and CS_2 along with other products as mentioned in the literature.[31] The thermal degradation of sodium poly(styrene 4-sulfonate) in the temperature range of 450–550 °C was observed due to polystyrene as well as $-SO_3Na$ group decomposition, while in the temperature range of 550–580 °C CO evolves along with an alcohol.[31] The total weight loss of compound **PSSTa** after complete degradation up to 700 °C was found to be 34.5%. The IR spectral analysis of the residual mass suggests the existence of oxidotantalate groups. The appearance of the bands at 1642 and 1124 cm^{-1} is indicative of sodium sulphate groups present in the residue.[31,32] Thus, TG-DTG analysis provides additional evidence in support of the composition and formula proposed for the title compounds.

Based on the above evidence, structures of the type schematically illustrated in Fig. 8 have been envisaged for complexes

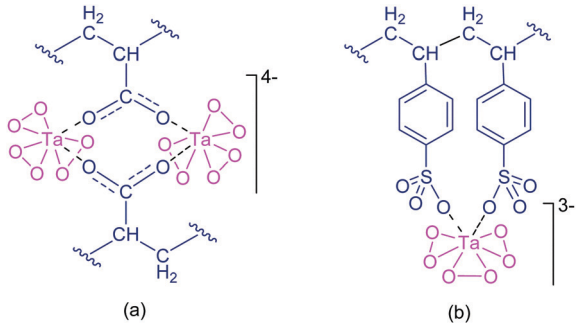

Fig. 8 Possible structures of (a) **PATa** and (b) **PSSTa**.

PATa and **PSSTa**. Three side-on bound η^2 peroxido groups in the co-ordination sphere are shown around each Ta(v) centre in each of the complexes. In the case of **PATa**, the carboxylate group of the poly(acrylate) chain binds to the metal in a bridged bidentate manner as has been observed in the case of previously reported poly(acrylate) supported peroxidometal complexes.[3c,9b] It is pertinent to mention that, in the majority of the structurally characterized pTa complexes reported so far,[1d,22,28c,33] the Ta atom exhibited a co-ordination number of eight. For complexes **PATa** and **PSSTa**, therefore, it is plausible that inter chain interactions between the seven co-ordinated triperoxidotantalum moieties and neighboring pendant carboxylate or sulphonate groups of the respective polymer chain would further complete eight-fold coordination around each Ta(v) centre and would provide stability to the polymer bound complexes. We have made similar observations earlier, in the case of peroxidoNb complexes anchored to WSPs.[3c,34]

Density functional studies

To further validate the feasibility of the proposed structures, we have performed theoretical investigations by employing the density functional theory (DFT) method for complex **PATa**. DFT calculations were carried out on the proposed model complex for **PATa**, shown in Fig. 8(a) at the PWC/DNP level of theory.[35] The optimized geometry of the complex is presented in Fig. 9, which shows two Ta(v) centres, each bonded to three η^2-peroxido groups and oxygen atoms of the carboxylate groups

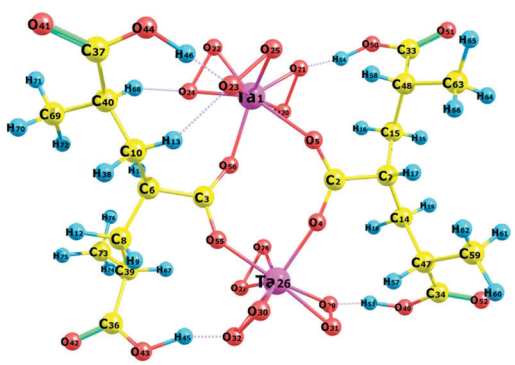

Fig. 9 Optimized structure of the **PATa** complex. The numbers represent the labeling of atoms as shown in Table 3. Colors: pink is tantalum, red is oxygen, yellow is carbon and blue balls represent hydrogen atoms.

in a bridging bidentate manner. Two of the bidentate peroxido groups are in a *cis* configuration, while the third one is in a *trans* position to the carboxylate groups of the polymer. The coordination polyhedron around the tantalum atom is a dodecahedron, as has been observed in the majority of the reported peroxidoTa complexes.[1d,28c,33a,c] It is important to note here that the H atoms of –COOH groups formed weak H-bonding with one of the O atoms of the metal bound peroxido ligands, which can also contribute in controlling the crystal packing.

The coordination distances calculated for complex **PATa** are within the range typical of heteroleptic peroxido complexes of tantalum(v).[28c,33a,c] Selected geometrical parameters such as bond lengths and bond angles of the complex obtained from DFT calculations are illustrated in Table 3. These theoretically obtained parameters are found to be in good accord with previously reported crystallographic parameters of heteroleptic peroxidotantalate or niobate complexes with a coordination environment comprising O-donor ligands.[1d,3b,c,28c,33a,36] We have further determined the vibrational frequency values for the optimized geometry of complex **PATa** and compared with the experimentally obtained data, as shown in Table S2 (ESI‡), which corroborate well with the theoretical values. However, some discrepancies are observed between the experimentally and theoretically obtained IR spectral values, but this is not unprecedented as such deviations are observed for vibrational bands of eight coordinated peroxidoTa complexes obtained from DFT based calculations.[22a,36c] Most importantly, the positive values of all calculated vibrational frequencies indicate that the optimized geometry of complex **PATa** is a stable structure.

Stability of the compounds toward decomposition in solution

Since the objective of the present study was to explore the biological attributes of pTa compounds, we considered it

Table 3 Selected bond lengths (Å) and bond angles (degrees) for the **PATa** complex calculated using the PWC/DNP level of theory

Structural index[a]	Calculated values	Structural index[a]	Calculated values
Ta1–O20	1.963	Ta26–O28	1.98154
Ta1–O21	2.019	Ta26–O29	2.06895
Ta1–O22	1.941	Ta26–O30	2.03100
Ta1–O23	2.043	Ta26–O31	1.96721
Ta1–O24	1.955	Ta26–O32	1.99647
Ta1–O25	1.959	Ta26–O4	2.05997
Ta1–O5	2.247	Ta26–O55	2.10322
Ta1–O56	2.067	O27–O28	1.45759
O20–O21	1.471	O29–O31	1.47133
O22–O24	1.475	O30–O32	1.45744
O23–O25	1.471	∠O20–Ta1–O21	43.3
O5–C2	1.251	∠O22–Ta1–O24	44.5
O56–C3	1.259	∠O23–Ta1–O25	43.1
O21–H54	1.32765	∠O5–Ta1–O56	72.6
O24–H68	1.94681	∠O4–Ta26–O55	83.935
O23–H46	1.33990	∠O27–Ta26–O28	43.895
O23–H13	1.99187	∠Ta1–O5–C2	144.509
O29–H53	1.28323	∠Ta1–O56–C3	144.242
O32–H45	1.31209	∠Ta26–O4–C2	164.284
Ta26–O27	1.91479	∠Ta26–O55–C3	138.855

[a] See Fig. 9 for atomic numbering.

necessary to ascertain the stability of these newly synthesized pTa compounds towards degradation in aqueous solution under different pH conditions since all the compounds are soluble in water. The stability of the pTa compounds was investigated at natural pH attained by dissolving the compounds in water. Moreover, the stability of the compounds was assessed under a wide range of pH values ranging from acidic to high pH (Fig. 10). The studies revealed that the peroxide content of all the tested peroxidotantalum compounds comprising monomeric tetraperoxidotantalate **TpTa** and polymer anchored pTa compounds **PATa** and **PSSTa** remained practically the same even after a period of 12 h. The observation indicated the stability of the compounds in aqueous solution under a wide range of pH values such as 1.2, 2.1, 3.1, 4.6, 7.0 and 8.0. Furthermore, ^{13}C NMR spectra of the compounds did not show any change in the spectral pattern when monitored over a period of 12 h [Fig. S1, ESI‡]. From this evidence, it has been confirmed that immobilized pTa compounds **PATa** and **PSSTa** retain their structural integrity and remain stable in solution under the tested reaction conditions. The title pV compounds *viz.* **PAV** and **PSSV** have already been reported to be stable in solution within a pH range of 3.6–8.0 over a period of 12 h.[9a,b] Thus, the observed stability of the compounds encouraged us to further explore their biochemical attributes.

Interaction of pTa compounds with catalase

Catalase is an enzyme that catalyzes disproportionation of H_2O_2 into water and molecular oxygen. Being a reactive oxygen species, hydrogen peroxide has long been known as a metabolic toxic waste product, responsible for DNA damage, and oxidative degradation of proteins and lipids, which ultimately leads to cell death.[37] During the last two decades, several groups have enormously contributed in changing this notion and have documented the significance of H_2O_2 as a key signal transducing agent modulating a variety of cellular processes.[38] However, its rapid decomposition in the presence of 'intracellular detoxifier' catalase and glutathione peroxidase has been the major caveat for studying its multiple cellular effects.[38a–d] Therefore, there have been efforts to find more stable peroxide derivatives that are less susceptible to degradation by peroxide scavenging enzymes, which would effectively substitute H_2O_2 at much lower concentration and replicate its actions. Previous studies have demonstrated that diperoxidovanadate (**DPV**), being nearly 50 times more stable to catalase *vis-a-vis* hydrogen peroxide,[9b,39] can substitute H_2O_2 in myriads of biological activities *viz.*, insulin-mimetic actions, cell proliferation, smooth muscle contraction, and also modulation of various signalling events.[38c,d,39] Subsequently, we have observed that macro complexes **PAV** and **PSSV**, obtained by anchoring of **DPV** to a WSP support, displayed even greater resistance to catalase compared to **DPV**, as revealed by their slower rates of peroxide loss under the effect of catalase (Table 4, entries 4–6).[9b] It is pertinent to mention that, like pV compounds, several of our synthesized pMo,[9b] pW[9e,40] and pNb[3b,9d] compounds were reported to display slower rates of degradation in the presence of catalase, while there are no available reports on the interaction of discrete pTa compounds with catalase.

The effects of catalase action on the newly synthesized polymer anchored pTa compounds as well as the precursor complex, **TpTa**, are shown in Fig. 10. Excellent ability of the pTa compounds to withstand catalase action is evident from the rates of peroxide loss from the compounds, ranging between 0.92 and 2.54 μM min^{-1} (Table 4, entries 1–3). These rates are *ca.* 5–6 times slower relative to the corresponding V containing analogues with similar ligand environments under the same reaction conditions (Table 4, entries 5 and 6). The trend observed for the title compounds is in the following order of increasing stability towards catalase: **PATa** > **PSSTa** > **TpTa**. Interestingly, a similar trend with respect to catalase resistance ability has also been displayed by the pV analogues, which could be arranged as **PAV** > **PSSV** > **DPV**. Thus, the free monomeric **DPV** as well as **TpTa** complexes are at least 50% less resistant to catalase action as revealed by their higher rates of peroxide loss relative to the respective polymer immobilized counterparts. These observations clearly demonstrate that immobilization of peroxidometallates on polymer supports imparts additional stability to the complexes. The extraordinary

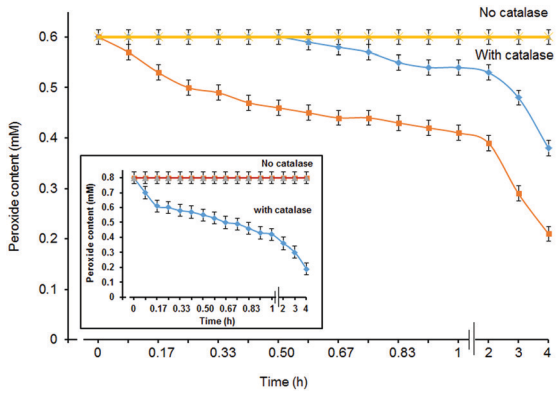

Fig. 10 Stability of compound **PATa** at different pH values: (▲) compound solution in distilled water, pH of the solution = 9.0, and (✕) solution of the complex in phosphate buffer (50 mM, pH 4.6). Stability of compound **TpTa** at different pH values: (▲) compound solution in distilled water, pH of the solution = 10.0, and (■) solution of the complex in phosphate buffer (50 mM, pH 4.6) (inset). Effect of catalase on (◆) **TpTa** (inset), (◆) **PATa** and (■) **PSSTa**. The reaction mixture contained phosphate buffer (50 mM, pH 7.0) and catalase enzyme (40 μg mL^{-1}) which was incubated at 30 °C for 5 min. The reaction was initiated after the addition of the respective compounds, and the peroxide content of aliquots drawn from the stock solution was determined at definite time intervals.

Table 4 Catalase dependant release of oxygen from the pV and pTa compounds

Entry	Compound	Concentration		Peroxide content (mM)	Loss of peroxide (μM min^{-1})
		mg mL^{-1}	(mM)		
1	**TpTa**	0.792	0.2	0.8	2.54
2	**PATa**	0.123	0.2	0.6	0.92
3	**PSSTa**	0.235	0.2	0.6	1.63
4	**DPV**[51]	0.034	0.2	0.4	12.00
5	**PAV**[9a]	0.11	0.2	0.4	5.80
6	**PSSV**[9b]	0.099	0.2	0.4	6.51

stability of the pTa compounds is further revealed by the loss of only one peroxido group from the triperoxidoTa species of complexes **PATa** and **PSSTa** in the presence of catalase, even after extending the reaction time up to 1 h, resulting in the formation of stable diperoxidoTa(v) in the presence of catalase as seen in Fig. 10. Interestingly, formation of diperoxidoTa(v) was also indicated in the case of the neat tetraperoxido complex **TpTa** by the loss of two peroxido groups under the effect of catalase. It is noteworthy that addition of catalase to peroxido compounds of V, Mo, and W resulted in a complete loss of peroxido groups within *ca.* 30 min of incubation,[9b,e,40,41] while pNb compounds showed a unique feature of retaining one peroxido group beyond a period of 1 h.[3b,9d] In the present study, the pTa compounds displayed a degradation pattern similar to peroxidoniobium complexes by retaining one of the peroxido groups even beyond 4 h.

According to a previous report, addition of catalase to a 0.1 mM solution of H_2O_2 resulted in rapid degradation at a rate of 430 μM min^{-1}, which led to its complete decomposition within *ca.* 2 min of reaction time.[39] On comparing this value to the rate of peroxide loss from the synthesized pTa compounds, it has been observed that the pTa compounds are nearly 200–400 times weaker as substrates to catalase compared to its native substrate, H_2O_2. Thus, these pTa complexes have emerged as the most resistant species towards catalase action among the synthetic peroxidometallate systems investigated so far.[3b,9b,d,e,40,41]

Effect of the pV and pTa complexes on the activity of acid phosphatase

The *in vitro* effect of pV containing macro complexes **PAV** and **PSSV** (Fig. 11b and c) and their Ta containing analogues **PATa** and **PSSTa** (Fig. 8) as well as free homoleptic complexes of the two metals *viz.*, **DPV** (Fig. 11a) and **TpTa** (Scheme 1) on the activity of ACP was investigated by employing an established assay system with *p*-NPP as a substrate.[3b,9c–e,19a,42] The dose dependent inhibition of the model enzyme by the tested complexes is depicted in Fig. 12. It is evident that with increasing inhibitor concentration the % ACP activity gradually decreases in the presence of each of the tested species. The inhibitory potential of each of the tested compounds was determined quantitatively from these plots by measuring the half maximal inhibitory concentration (IC_{50}). The IC_{50} values, which represent 50% suppression of the actual enzyme activity, are presented in Table 5. The IC_{50} values for the pTa compounds were recorded to be in the range of 0.3–5.1 μM, while for the pV compounds they were in the range of 1–17 μM. These data demonstrate that each of the tested pV and pTa complexes actively inhibits ACP function even at very low compound concentration. However, the IC_{50} values clearly show that the peroxidotantalum complexes are 2–3 fold more potent inhibitors compared to the respective pV analogues.

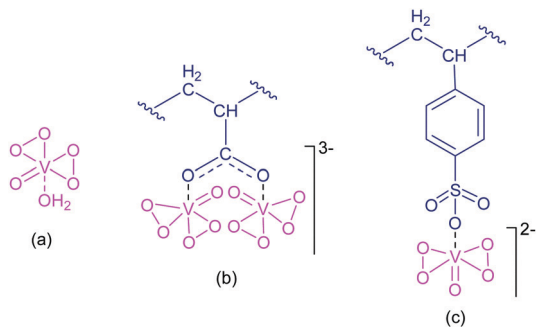

Fig. 11 Peroxido compounds of vanadium(v) under investigation for the present study: (a) **DPV**, (b) **PAV**, and (c) **PSSV**.

On comparing the IC_{50} values of the pV macro complexes with the monomeric **DPV** (Table 5, entries 4–6), the compounds could be arranged in the following order of potency – **PSSV** > **PAV** > **DPV**, whereas the pTa complexes showed the following trend: **PSSTa** > **TpTa** > **PATa**. The relatively higher inhibitor efficiency displayed by the free monomeric **TpTa** may possibly be correlated to the presence of four η^2-peroxido ligands in the co-ordination sphere of this holmoleptic tetraperoxidotantalate complex. Moreover, in the case of **TpTa** (Fig. 12b), after the initial suppression of the ACP activity to *ca.* 60% with a 1.0 μM concentration of the inhibitor, an abrupt decrease in ACP activity was noted on a further increase of the **TpTa** concentration to 1.5 μM, resulting in non-linearity of the plot. The exact cause of this observation is however not clear at this stage. An interesting common feature revealed by these trends is the remarkable inhibitor efficiency displayed by the macro complexes **PSSV** and **PSSTa** bound to polymer PSS. In fact, **PSSTa** has been found to be the most potent inhibitor with its sub-micromolar IC_{50} value as low as 0.34 μM. The observation is consistent with previous findings from our laboratory showing PSS anchored peroxidoniobium and peroxidotungsten complexes as the most effective inhibitors of ACP.[9c–e] Since individually neither the pristine polymers nor H_2O_2 had any observable effect on ACP function, it can safely be inferred that the inhibitor activity of the test compounds originates from the interaction of the intact metal complexes with the enzyme. It is also evident from these observations that the nature of the co-ligand environment affects the inhibitory ability of the tested species substantially.

Kinetics of ACP inhibition by the pV and pTa compounds

Enzyme kinetics investigation is a major implement for distinguishing between different modes of inhibition of enzyme catalyzed reactions such as competitive, non-competitive or mixed type inhibition. Therefore, in order to elucidate the mode of the observed inhibitory effect displayed by the pV and pTa complexes, the steady state kinetics of the ACP catalyzed hydrolysis of *p*-NPP was investigated. The kinetic parameters, K_m and V_{max}, were determined from the Lineweaver–Burk double reciprocal plots[42b,43] where the reciprocal initial velocity was plotted against the reciprocal substrate concentration in the absence or presence of the inhibitor species at different concentrations, as shown in Fig. 13 and Fig. S2 (ESI‡). The kinetic measurements for the pV and pTa compounds including the free monomeric (**DPV** and **TpTa**) as well as the polymer anchored compounds (**PAV**, **PSSV**, **PATa** and **PSSTa**) produced straight lines which intercepted at a point in close proximity to

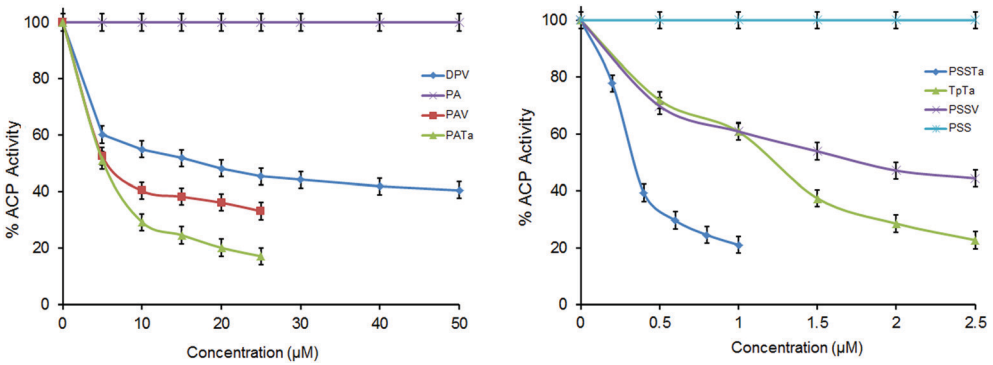

Fig. 12 The effect of neat homoleptic and polymer anchored peroxidometal compounds as well as the free ligand on the activity of ACP. The ACP catalyzed rates of hydrolysis of *p*-NPP at pH 4.6 were determined at 30 °C by measuring A_{405} in a reaction mixture comprising ACP (18.38 μg mL^{-1}) and *p*-NPP (2 mM) in acetate buffer (0.1 M, pH = 4.6) in the absence or presence of the stated concentrations of the inhibitors. (a) For **DPV** and the free ligand poly(sodium acrylate) (PA), the concentrations are: 5, 10, 15, 20, 25, 30, 40 and 50 μM, and for **PAV** and **PATa**, compound concentration: 5, 10, 15, 20 and 25 μM, and (b) for **PSSV**, **TpTa** and the free ligand poly(sodium 4-styrene sulfonate) (PSS), compound concentration: 0.5, 1, 1.5, 2.0 and 2.5 μM, and for **PSSTa**, the compound concentrations are: 0.2, 0.4, 0.6, 0.8 and 1.0 μM. The data are presented as the means ± SE from three separate experiments. For polymeric compounds, the compound concentrations are on the basis of the peroxidometal loading.

Table 5 Half-maximal inhibitory concentration (IC_{50}) and inhibitor constant (K_i and K_{ii}) values for the pV and pTa compounds

Entry	Compound	IC_{50} (μM)	K_i (μM)	K_{ii} (μM)	K_{ii}/K_i	Types of inhibition
1	**TpTa**	1.77	0.94	0.91	0.97	Non-competitive inhibition
2	**PATa**	5.06	2.00	2.20	1.10	Non-competitive inhibition
3	**PSSTa**	0.34	0.16	0.17	1.06	Non-competitive inhibition
4	**DPV**	16.79	4.71	4.70	0.99	Non-competitive inhibition
5	**PAV**	5.64	2.50	2.50	1.00	Non-competitive inhibition
6	**PSSV**	1.22	0.82	0.82	1.00	Non-competitive inhibition

Note: ACP catalyzed rates of hydrolysis of *p*-NPP at pH 4.6 were determined at 30 °C by measuring A_{405} in a reaction mixture containing ACP (18.38 μg mL^{-1}) and *p*-NPP (50–300 μM) in acetate buffer (0.1 M, pH 4.6) in the presence of the stated concentrations of the inhibitors.

the 1/[S] axis. From these plots it is evident that with increasing concentration of the inhibitor species the value of velocity V_{max} decreased, whereas the K_m value remained constant. This suggested a non-competitive mode of inhibition for each of the tested inhibitor species.

To ascertain the affinity of the enzyme for the inhibitor species, we have also determined the inhibitor constants, K_i and K_{ii}. Inhibitor constant K_i is the measure of the inhibitor's affinity to the free enzyme, which was obtained from the *x*-intercepts of the secondary plot of the slope of the primary L–B plot *versus* the inhibitor concentration, as shown in Fig. 13 and Fig. S2 (ESI‡) [inset (a)]. Whereas, constant K_{ii} reveals the inhibitor's affinity for the enzyme–substrate complex, determined from the re-plot of the intercepts of the primary L–B plot against the inhibitor concentration with the *x*-intercept of this graph being equivalent to K_{ii} [Fig. 13 and Fig. S2 (ESI‡), inset (b)]. The values of K_i and K_{ii} for each of the inhibitor species are listed in Table 5. The inhibitory constant for the competitive part of inhibition K_i values for the tested inhibitor compounds was found to be comparable to the inhibitor constant for the non-competitive part of inhibition K_{ii} with the ratio of the K_{ii}/K_i values being close to unity. These observations are typical of a non-competitive inhibitor and are in accord with the mechanism of inhibition displayed by other polymer bound peroxidometallates reported previously from our laboratory.[3b,9b–e] The trend in inhibition potency of the pV and pTa compounds revealed by the kinetic measurements (Table 5) has been found to be consistent with that obtained from their IC_{50} values.

A non-competitive inhibitor usually binds to the enzyme reversibly at a site far removed from the active site, which causes an alteration in the overall three dimensional shape of the enzyme leading to reduced activity of the enzyme.[3b,9c] A non-competitive inhibitor has the same affinity for both the enzyme and the enzyme–substrate complex. Phosphatases, in general, are known to be inhibited by smaller oxyanions of V, Mo and W with penta or hexa co-ordinated structures in a competitive manner, as these ions share a structural analogy with phosphate.[3b,9b,c,15,44] However, in the case of acid phosphatases, different oxidometal ions inhibited the ACP function *via* diverse pathways ranging from competitive and non-competitive to uncompetitive modes.[3b,9c,44a–c,45] For example, Fei *et al.*[19a] reported molybdate and vanadate to be un-competitive and non-competitive inhibitors of wheat thylakoid acid phosphatase, respectively, whereas Das *et al.*[9c] also observed a non-competitive mode of inhibition of ACP by tungstate. Averill and his co-workers reported tungstate and molybdate as non-competitive inhibitors of bovine spleen purple acid phosphatase.[46] This information suggested different mechanistic preferences for different oxidometal ions in inhibition of acid phosphatase, in spite of having similar structural characteristics. It is however notable that reports pertaining to ACP inhibition by peroxidometallates are still very scarce, in spite of the extensive studies on peroxidovanadate systems in inhibition of phosphohydrolases.

Acid phosphatase, isolated from various sources *viz.* human prostate, wheat germ, and plants, possesses dinuclear iron at the active site with a histidine residue and a highly conserved amino acid sequence.[19a,45–47] It is relevant to recall here the work of Averill and his co-workers, wherein oxyanions such as

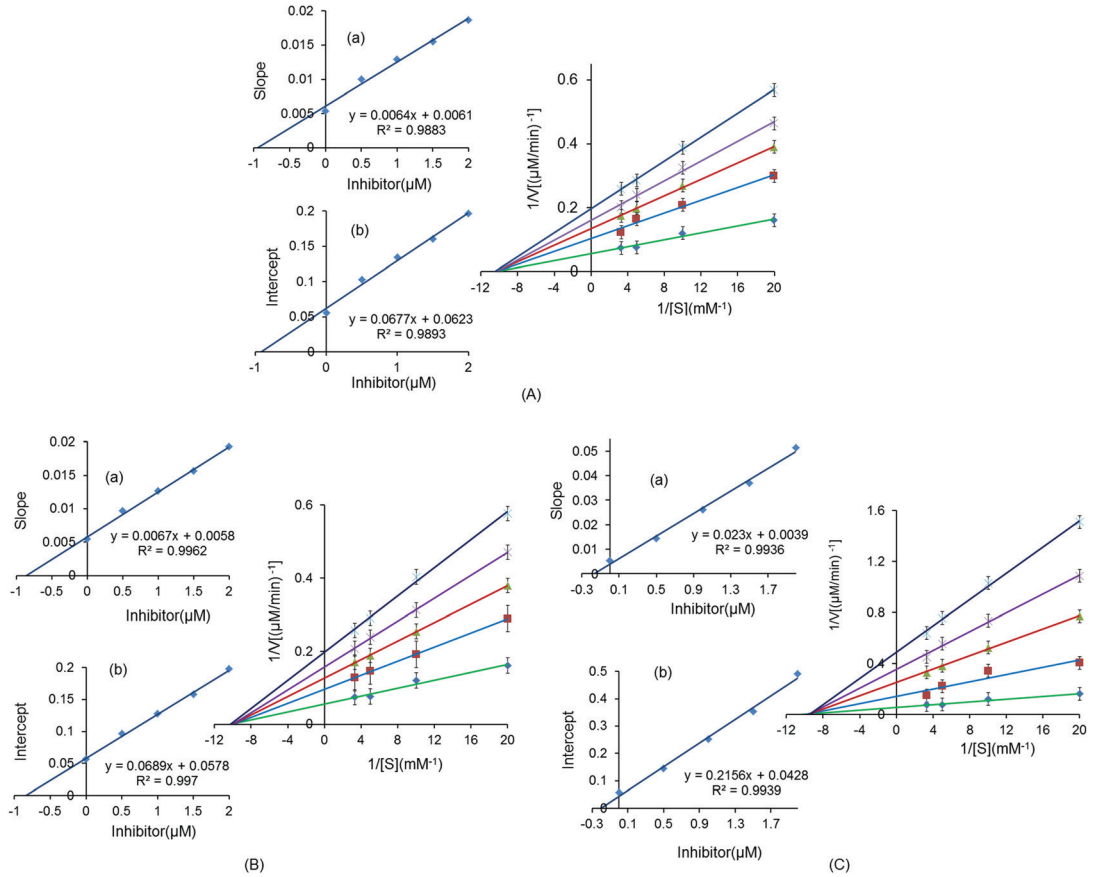

Fig. 13 Lineweaver–Burk plots for the inhibition of ACP activity in the presence or absence of (A) **TpTa**, (B) **PSSV** and (C) **PSSTa**. The inset presents the secondary plot of the initial kinetic data of the Lineweaver–Burk plot. The reaction mixture contained acetate buffer (0.1 M, pH 4.6) and *p*-NPP (50–300 μM). The reaction was started by adding ACP (18.38 μg mL^{-1}) to the reaction solution, which was pre-incubated for 5 min, and the rates of hydrolysis in the presence of ◆ 0 μM, ■ 0.5 μM, ▲ 1.5 μM, × 2 μM, and ✳ 2.5 μM inhibitors were obtained. The values are expressed as the mean ± SE from three separate experiments. Inset: (a) The slopes were plotted against the inhibitor concentrations and K_i values were obtained from the *x*-intercepts of these re-plots. (b) The vertical intercepts were plotted against the inhibitor concentration and K_{ii} values were obtained from the *x*-intercepts of these re-plots.

molybdate and tungstate, presumably because of their larger size, induce non-competitive inhibition of bovine spleen purple acid phosphatase by binding the two iron atoms in the binuclear active site of the enzyme in a bridging manner.[46] The peroxidometal derivatives examined in the present study possibly inhibit the ACP function in a non-competitive manner as they are unlikely to bind to the enzyme active site as a transition state analogue due to their larger size.[9b–e] Additionally, as has been demonstrated by Fei *et al.*, the enzyme could be inactivated by highly oxidative species *via* oxidative transformation of the Fe^{2+} centre in the active site of the enzyme to its ferric form resulting in non-competitive inhibition of the enzyme.[19a] According to previous literature, peroxidovanadate exerted an inhibitory effect on tyrosine phosphatase by oxidizing the cysteine residue in the catalytic domain of the enzyme.[11,48] Taking into account these important findings, the observed non-competitive inhibition by the pV and pTa compounds in the present study may safely be attributed to their oxidative interaction with either the Fe^{2+} centre in the active site or oxidation prone –SH groups of the protein chain. Such groups play a crucial role in stabilization of the quaternary structure and are essential for enzyme activity.[9c,19a] It is reasonable to expect a redox interaction between the inhibitor complexes and the enzyme as the compounds examined herein were also found to actively facilitate oxidation of organic substrates.[9a,49] However, in the absence of direct evidence and considering the complexity of the involved biological process, it is somewhat difficult to draw any definite conclusion regarding the exact mechanism of inhibition by the tested compounds. Further investigation in this respect will evidently be necessary to unravel the actual mechanism of the observed inhibition. Nevertheless, the existence of substantial reports on phosphatase inhibitory ability of pV compounds offers adequate credibility to our proposed hypothesis.

Conclusion

In summary, we have introduced a set of water soluble, structurally defined pTa complexes immobilized on non-cross linked, linear soluble polymer matrices. The spectral analysis data, substantiated by the results of DFT studies, provided satisfactory evidence for the mode of coordination of the pendant ligands to the Ta(v) centre and the composition of the macro complexes. The anchored pTa

compounds, like their pV analogues, remain hydrolytically stable in a wide range of pH values including at acidic pH. Importantly, the pTa compounds displayed extraordinary stability in the presence of catalase, by partially retaining the co-ordinated peroxido groups even beyond 4 h of incubation with the enzyme. In contrast, complete loss of peroxido groups from peroxidovanadate compounds occurred under catalase action within *ca.* 30 min of incubation.[9b,41] Furthermore, our experiments establish that, although the tested complexes of both Ta(v) and V(v) exert strong inhibitory effects on ACP, the pTa derivatives showed greater efficiency, at nearly a 2–3 fold lesser dose, than the corresponding pV compounds. Detailed enzyme kinetic analysis results demonstrated that the pV and pTa compounds exhibit a distinct mechanistic preference to inhibit the enzyme function *via* a non-competitive pathway, as has been observed in the case of phosphatase inhibition induced by several other polymer bound peroxidometallates reported previously by us.[9b–d] Thus, it may be expected that our findings will provide a facile route to the design of potent peroxidometallate based inhibitor systems which may serve as selective probes of non-competitive sites of phosphatases.

Experimental

Materials and methods

All reagent grade chemicals were used to carry out this work. The sources of the chemicals are given below: vanadium pentoxide (SRL), hydrogen peroxide, acetone and sodium thiosulphate (RANKEM), potassium dichromate, sulfuric acid and sodium hydroxide (E. Merck, India), boric acid, sodium bicarbonate and potassium iodide (SRL), and tantalum pentoxide, poly(sodium acrylate) (M_w = 2100), poly(sodium 4-styrene sulfonate) (M_w = 200 000), acid phosphatase from wheat thylakoid membrane (ACP), catalase, and *p*-nitrophenyl phosphate (*p*-NPP) (Sigma-Aldrich Chemical Company, Milwaukee, USA). The preparation of $Na[VO(O_2)_2(H_2O)]$ (**DPV**),[50] $[V_2O_2(O_2)_4(carboxylate)]$–PA [PA = poly(sodium acrylate)] (**PAV**)[9a] and $[VO(O_2)_2(sulfonate)]$–PSS [PSS = poly(sodium 4-styrene sulfonate)] (**PSSV**)[9b] was performed on the basis of the methods reported earlier by our laboratory. Distilled and deionized water was used for solution preparation.

The tantalum content in the synthesized compounds was estimated by inductively coupled plasma-optical emission spectroscopy (ICP-OES). The composition of the compounds was also confirmed from EDX analysis. The amounts of C, H and N in the synthesized compounds were determined by using a PerkinElmer 2400 series II elemental analyzer. To measure the peroxide amount in the compounds volumetrically, the iodometric method was used where a weighed amount of the compound was added to a cold solution of 1.5% boric acid (w/v) in 0.7 M sulfuric acid (100 mL) and titrated with standard sodium thiosulfate solution.[51]

The IR spectral analysis of the samples was carried out by using a PerkinElmer spectrum 100 FTIR spectrophotometer. The Raman spectra of the compounds were recorded on an EZ Raman-N (Enwaveoptronics), equipped with a diode laser with an excitation wavelength of 785 nm and a laser maximum output power of 350 mW. The parameters of the measurement were a 10 s exposure time, 5 accumulations, a laser power 10% of the output power and a 100× objective and the pixel resolution was set to 1.44 cm^{-1} per pixel. The UV-vis absorption spectra in solution were recorded using a Cary model Bio 100 spectrophotometer, equipped with a peltier controlled constant temperature cell, in 1 cm quartz cuvettes. Thermogravimetric analysis (TGA) was done on a SHIMADZU TGA-50 system at a heating rate of 10 °C min^{-1} under a N_2 atmosphere using an aluminium pan. A JEOL JSM-6390LV scanning electron microscope attached to an energy-dispersive X-ray detector was used to carry out scanning electron microscopy (SEM) and energy-dispersive X-ray analysis of the compound. Scanning was performed in the 1–20 μM range, and images were taken at a magnification of 15–20 kV. Data were obtained using INCA software. Standardization of the data analysis is an important part of the SEM-EDX instrument. The ^{13}C NMR spectra of the compounds were recorded with a JEOL JNM-ECS 400 spectrometer at a carbon frequency of 100.5 MHz, 32 768 X-resolution points, number of scans 8000–20 000, 1.04 s acquisition time and 2.0 s relaxation delay with the ^1H NMR decoupling method in D_2O as a solvent. Magnetic susceptibilities of the complexes were measured with the help of the Gouy method, using Hg[Co(NCS)] as the calibrant.

Preparation of sodium tetraperoxidotantalate, $Na_3[Ta(O_2)_4]\cdot H_2O$ (TpTa)

Precursor $Na_3[Ta(O_2)_4]\cdot H_2O$ was prepared by the following reported method[1d,52] – 1 g of tantalum oxide (Ta_2O_5) was fused with 1.6 g of NaOH in a nickel crucible at 700 °C for 3 hours. The fused product was then cooled and dissolved in about 70 mL of 1 M 30% H_2O_2. The solution was then filtered to remove the unreacted Ta_2O_5 and kept in ice cold conditions. After 12 hours, tetraperoxidotantalate crystals were obtained.

Synthesis of $[Ta_2(O_2)_6(carboxylate)_2]$–PA (PATa)

The reaction procedure developed for the synthesis of **PATa** consisted of gradual addition of 10 mL 30% H_2O_2 (88.49 mmol) to a mixture of the precursor complex sodium tetraperoxidotantalate $Na_3[Ta(O_2)_4]\cdot H_2O$ (1.4 g, 3.56 mmol) with 1 g of polymer PA dissolved in a minimum volume of water. The pH of the reaction solution was recorded to be *ca.* 7.0. Dilute HNO_3 (4 M) was added drop-wise to the system until the pH was lowered to *ca.* 6.0. The reaction mixture was allowed to stand for about 3 h in an ice-bath. The temperature was maintained below 4 °C throughout the procedure. Then, pre-cooled acetone was added to it to induce precipitation under continuous stirring. The supernatant liquid was decanted off and the residue was treated repeatedly with acetone to obtain the desired microcrystalline product, which was separated by centrifugation.

Found: C, 18.2; H, 1.7; O, 35.3; Na, 14.9; Ta, 31.2; O_2^{2-}, 15.7. The metal loading calculated from the obtained tantalum content is 1.62 mmol g^{-1} of the polymer.

Synthesis of $[Ta(O_2)_3(sulfonate)_2]$–PSS (PSSTa)

The methodology for the synthesis of **PSSTa** is as follows – sodium tetraperoxidotantalate $Na_3[Ta(O_2)_4]\cdot H_2O$ (0.22 g, 0.57 mmol) was solubilized in 4 mL of 30% H_2O_2 (35.2 mmol) in the presence of the polymer, PSS (2 mL). The pH of the reaction solution was found to be *ca.* 5.8, which was adjusted to *ca.* 6.0 by the addition of NaOH. The system was allowed to stand while maintaining the temperature below 4 °C. Pre-cooled acetone was added under vigorous stirring to induce precipitation. Similarly to mentioned in the synthesis of **PATa**, the supernatant liquid was decanted off and the residue was washed repeatedly with acetone to obtain the microcrystalline product. The obtained products were dried *in vacuo* over concentrated sulphuric acid and stored for several weeks.

Found: C, 33.5; H, 2.6; O, 28.3; Na, 12.0; S, 12.1; Ta, 15.3; O_2^{2-}, 8.1. The metal loading on the polymer was calculated to be 0.85 mmol g^{-1} of the polymer on the basis of the metal content obtained from elemental analysis.

Stability of the pTa compounds in aqueous solution

To determine the stability of the compounds in solution, a stock solution of 0.2 mM concentration (100 mL) was prepared for each of the compounds by dissolving a weighed amount of the respective compounds **TpTa** (0.792 mg mL^{-1}), **PATa** (0.123 mg mL^{-1}) and **PSSTa** (0.235 mg mL^{-1}) in water. The peroxide content in aliquots drawn from the stock solution was determined at different time intervals for a period of 12 h by the procedure described earlier in Section 2.1. The stability of the compounds was measured similarly at different pH values – pH 4.6, pH 7.0 and pH 8.0 maintained by using phosphate buffer (50 mM), pH 1.2 and pH 2.1 (50 mM KCl/HCl buffer), and pH 3.1 (50 mM citrate buffer). Moreover, ^{13}C NMR spectra of the compounds were monitored over a period of 12 h for any possible change. For the polymer anchored pTa compounds, the compound concentrations were calculated on the basis of the actual peroxidotantalum loading (mmol g^{-1}).

Effect of catalase on the pTa complexes

The extent of decomposition of the synthesized pTa compounds in the presence of catalase was measured by determining the peroxide content of the compounds in a solution at specified time intervals. The tested reaction mixture contained phosphate buffer (50 mM, pH 7.0) and the enzyme (40 μg mL^{-1}), incubated at 30 °C. The total volume of the reaction solution was kept at 100 mL. The reaction was initiated after the addition of the weighed amount of pTa compounds (as mentioned in Table 4) to the pre-incubated solution. Aliquots of 5 mL reaction solution were pipetted out at an interval of 5 min and the loss of peroxide amount was determined by iodometric titration of the solution after quenching the reaction by adding it to cold sulfuric acid (0.7 M, 100 mL).

Method of acid phosphatase activity measurement

The activity of acid phosphatase was measured spectrophotometrically by using *p*-nitrophenyl phosphate (*p*-NPP) as a substrate.[3b,9c,19a,42] In the standard protocol, the reaction mixture contained the enzyme (18.38 μg protein mL^{-1}) and different concentrations of the inhibitor species [the concentration varies between 5 and 50 μM for **DPV**, 5 and 25 μM for **PAV** and **PATa**, 0.5 and 2.5 μM for **TpTa** and **PSSV**, and 0.2 and 1.0 μM for **PSSTa** as shown in Fig. 12] in acetate buffer (0.1 M, pH = 4.6). For the polymer anchored complexes, concentrations were calculated on the basis of the metal loading (mmol g^{-1}). The reaction was started by the addition of *p*-NPP to the reaction mixture, which was pre-incubated for 5 min at 30 °C. After 30 min of incubation, the reaction was terminated by adding 0.9 mL of 0.5 M NaOH solution. The release of *p*-nitrophenol from the substrate was determined by measuring the absorbance of the reaction solution at 405 nm (molar extinction co-efficient of *p*-nitrophenolate = 18 000 M^{-1} cm^{-1}).[53] The enzyme activity in the absence of the inhibitors was used as a control. The half-maximal inhibitory concentration (IC_{50}) values were determined graphically giving 50% inhibition of the enzyme. All the experiments were performed in triplicate. The data in the figures were presented as the average ± SE from three separate experiments.

Determination of kinetic parameters

The kinetic studies were carried out by using a substrate concentration in the range of 50–300 μM in the presence or absence of each of the inhibitor species with varied concentrations as shown in Fig. 13 and Fig. S2 (ESI‡). The kinetic constants, maximum velocity (V_{max}) and Michaelis constant (K_m) were determined from Lineweaver–Burk plots by rearranging the Michaelis–Menten equation.[42b,43]

$$\frac{1}{V} = \frac{K_m}{V_{max}[S]} + \frac{1}{V_{max}} \quad (1)$$

In the present case, expression (2) was used to determine the rate of the reaction

$$V = \left\{ \frac{V_{max} \times [S]}{K_m\left(\frac{1+[I]}{K_i}\right) + [S]\left(\frac{1+[I]}{K_{ii}}\right)} \right\} \quad (2)$$

where V is the velocity, [S] is the *p*-NPP concentration and [I] refers to the inhibitor concentration. K_i and K_{ii} are the inhibitory constants for the competitive and non-competitive part, respectively. They were determined from the secondary plots of the initial rate data by linear regression analysis. The K_i value was obtained from the *x*-intercepts of the re-plots where the slopes from the L–B plots were plotted against the inhibitor concentration. The K_{ii} value was also determined from the *x*-intercepts of the plots of intercepts that were obtained from Lineweaver plots against the inhibitor concentration.

Computational details

Theoretical calculations were performed using the density functional theory (DFT) method with the DMol^3 package.[35a] We have utilized the Local Density Approximation (LDA) using the Harris and Perdew–Wang (PWC) local functional[35b] combined with the double numerical polarized (DNP) basis set

to obtain the optimized electronic structure of complex **PATa**. The optimized structure of **PATa** is shown in Fig. 9. We have further performed frequency calculations on the **PATa** complex to obtain the various modes of vibration of the complex by using the same level of theory.

Author contributions

The contributions of the authors in the research article are listed as follows: Gangutri Saikia (data curation, lead; formal analysis, lead; funding acquisition, equal; investigation, lead; methodology, equal; project administration, equal; resources, supporting; validation, equal; visualization, equal; writing – orginal draft, equal), Hiya Talukdar (formal analysis, supporting; investigation, supporting), Kabirun Ahmed (formal analysis, supporting), Nand Kishor Gour (formal analysis, supporting), Nashreen S. Islam (conceptualization, lead; funding acquisition, equal; methodology, equal; project administration, equal; resources, lead; supervision, lead; validation, equal; visualization, equal; writing – original draft, equal).

Conflicts of interest

There are no conflicts to declare.

Acknowledgements

Financial support from Department of Science and Technology, New Delhi, India, under the Women Scientist Scheme-A (WOS-A) project (Grant No. SR/WOS-A/CS-35/2017), is gratefully acknowledged.

References

1 (*a*) R. A. Sheldon and J. K. Kochi, *Metal Catalyzed Oxidations of Organic Compounds*, Academic Press, New York, 1981; (*b*) V. Conte and O. Bortolini, in *PATAI'S Chemistry of Functional Groups*, ed. I. Marek, John Wiley & Sons, New York, 2009, pp. 1–76; (*c*) D. C. Crans, *J. Org. Chem.*, 2015, **80**, 11899; (*d*) D. Bayot and M. Devillers, *Coord. Chem. Rev.*, 2006, **250**, 2610; (*e*) O. Bortolini and V. Conte, *J. Inorg. Biochem.*, 2005, **99**, 1549; (*f*) T. Ramasarma, *Proc. Indian Natl. Sci. Acad., Part B*, 2003, **69**, 649; (*g*) S. Treviño, A. Díaz, E. Sánchez-Lara, B. L. Sanchez-Gaytan, J. M. Perez-Aguilar and E. González-Vergara, *Biol. Trace Elem. Res.*, 2019, **188**, 68; (*h*) R. R. Langeslay, D. M. Kaphan, C. L. Marshall, P. C. Stair, A. P. Sattelberger and M. Delferro, *Chem. Rev.*, 2018, **119**, 2128; (*i*) J. C. Pessoa, S. Etcheverry and D. Gambino, *Coord. Chem. Rev.*, 2015, **301**, 24.

2 (*a*) H. Thomadaki, A. Lymberopoulou-Karaliota, A. Maniatakou and A. Scorilas, *J. Inorg. Biochem.*, 2011, **105**, 155; (*b*) G. S. Kim, D. A. Judd, C. L. Hill and R. F. Schinazi, *J. Med. Chem.*, 1994, **37**, 816.

3 (*a*) G. Fraqueza, C. A. Ohlin, W. H. Casey and M. Aureliano, *J. Inorg. Biochem.*, 2012, **107**, 82; (*b*) S. R. Gogoi, G. Saikia, K. Ahmed, R. Duarah and N. S. Islam, *Polyhedron*, 2017, **121**, 142; (*c*) G. Saikia, S. R. Gogoi, J. J. Boruah, B. M. Ram, P. Begum, K. Ahmed and N. S. Islam, *ChemistrySelect*, 2017, **2**, 5838.

4 (*a*) V. K. Balla, S. Bodhak, S. Bose and A. Bandyopadhyay, *Acta Biomater.*, 2010, **6**, 3349; (*b*) T. Beline, J. H. da Silva, A. O. Matos, N. F. A. Neto, A. B. de Almeida, F. H. N. Júnior, D. M. G. Leite, E. C. Rangel and V. A. Barão, *Mater. Sci. Eng., C*, 2019, **101**, 111; (*c*) H. Qian, T. Lei, P. Lei and Y. Hu, *Tissue Eng., Part B*, 2021, **27**(2), 166; (*d*) J. Ma, Y. Sun, R. Zan, J. Ni and X. Zhang, *Mater. Sci. Eng., C*, 2020, **109**, 110520; (*e*) H. Qian, T. Lei, Z. Ye, Y. Hu and P. Lei, *BioMed Res. Int.*, 2020, **2020**, 1; (*f*) E. Uslu, H. Öztatlı, B. Garipcan and B. Ercan, *J. Biomed. Mater. Res., Part B*, 2020, **108**(7), 2743.

5 (*a*) G. Mohandas, N. Oskolkov, M. T. McMahon, P. Walczak and M. Janowski, *Acta Neurobiol. Exp.*, 2014, **74**, 188; (*b*) E. C. Gee, R. Jordan, J. A. Hunt and A. Saithna, *J. Mater. Chem. B*, 2016, **4**, 1020; (*c*) H. L. Huang, M. T. Tsai, Y. J. Lin and Y. Y. Chang, *Thin Solid Films*, 2019, **688**, 137268; (*d*) N. George and A. B. Nair, *Fundamental Biomaterials: Metals*, Woodhead Publishing, UK, 2018.

6 (*a*) Y. Jin, X. Ma, S. Zhang, H. Meng, M. Xu, X. Yang and J. Tian, *Cancer Lett.*, 2017, **397**, 61; (*b*) X. Hu, Y. Wang and M. Xu, *Int. J. Biol. Macromol.*, 2019, **135**, 501.

7 P. Štarha, Z. Trávníček and Z. Dvořák, *Chem. Commun.*, 2018, **54**, 9533.

8 D. Hatzipanayioti and K. Kontotheodorou, *Spectrochim. Acta, Part A*, 2011, **78**, 949.

9 (*a*) D. Kalita, S. Sarmah, S. P. Das, D. Baishya, A. Patowary, S. Baruah and N. S. Islam, *React. Funct. Polym.*, 2008, **68**, 876; (*b*) J. J. Boruah, D. Kalita, S. P. Das, S. Paul and N. S. Islam, *Inorg. Chem.*, 2011, **50**, 8046; (*c*) S. P. Das, S. R. Ankireddy, J. J. Boruah and N. S. Islam, *RSC Adv.*, 2012, **2**, 7248; (*d*) S. R. Gogoi, PhD thesis, Tezpur University, 2017; (*e*) S. P. Das, PhD thesis, Tezpur University, 2012.

10 N. Chatterjee, T. Anwar, N. S. Islam, T. Ramasarma and G. Ramakrishna, *Mol. Cell. Biochem.*, 2016, **420**, 9.

11 V. Khanna, M. Jain, M. K. Barthwal, D. Kalita, J. J. Boruah, S. P. Das, N. S. Islam, T. Ramasarma and M. Dikshit, *Pharmacol. Res.*, 2011, **64**, 274.

12 P. Schwendt, J. Tatiersky, L. Krivosudský and M. Šimuneková, *Coord. Chem. Rev.*, 2016, **318**, 135.

13 (*a*) A. Skorobogaty and T. D. Smith, *Coord. Chem. Rev.*, 1984, **53**, 55; (*b*) B. Schechter, R. Arnon and M. Wilchek, *React. Polym.*, 1995, **25**, 167; (*c*) J. Jagur-Grodzinski, *React. Funct. Polym.*, 1999, **39**, 99.

14 A. Y. Louie and T. J. Meade, *Chem. Rev.*, 1999, **99**, 2711.

15 C. C. McLauchlana, B. J. Petersb, G. R. Willsky and D. C. Crans, *Coord. Chem. Rev.*, 2015, **301**, 163.

16 (*a*) J. L. McConnell and B. E. Wadzinski, *Mol. Pharmacol.*, 2009, **75**, 1249; (*b*) A. R. Saltiel, *Cell*, 2001, **104**, 517.

17 D. Gambino, *Coord. Chem. Rev.*, 2011, **255**, 2193.

18 D. C. Crans, J. J. Smee, E. Gaidamauskas and L. Yang, *Chem. Rev.*, 2004, **104**, 849.

19 (*a*) M. J. Fei, J. S. Chen and X. Y. Wang, *J. Integr. Plant Biol.*, 2006, **48**, 294; (*b*) W. N. Lipscomb and N. Sträter, *Chem. Rev.*, 1996, **96**, 2375; (*c*) D. E. Wilcox, *Chem. Rev.*, 1996, **96**, 2435.

20 (*a*) B. L. Rivas, E. D. Pereira and I. Moreno-Villoslada, *Prog. Polym. Sci.*, 2003, **28**, 173; (*b*) B. L. Rivas, E. D. Pereira, M. Palencia and J. Sánchez, *Prog. Polym. Sci.*, 2011, **36**, 294.
21 (*a*) B. L. Rivas and I. Moreno Villoslada, *J. Appl. Polym. Sci.*, 1998, **70**, 219; (*b*) B. L. Rivas and I. Moreno-Villoslada, *Chem. Lett.*, 2000, 166.
22 (*a*) D. Bayot, M. Devillers and D. Peeters, *Eur. J. Inorg. Chem.*, 2005, 4118; (*b*) G. Haxhillazi and H. Haeuseler, *J. Solid State Chem.*, 2004, **177**, 3045.
23 K. Nakamoto, *Infrared and Raman spectra of inorganic and coordination compounds, Part B*, Wiley and Sons, New York, 1997.
24 (*a*) C. Djordjevic, M. Lee and E. Sinn, *Inorg. Chem.*, 1989, **28**, 719; (*b*) P. Schwendt, P. Švančárek, L. Kuchta and J. Marek, *Polyhedron*, 1998, **17**, 2161; (*c*) H. Li and C. P. Tripp, *Langmuir*, 2004, **20**, 10526.
25 (*a*) B. L. Rivas, G. V. Seguel and K. E. Geckeler, *J. Appl. Polym. Sci.*, 2002, **85**, 2546; (*b*) A. Pourjavadi and H. Ghasemzadeh, *Polym. Eng. Sci.*, 2007, **47**, 1388.
26 (*a*) P. J. Cordeiro and T. D. Tilley, *Langmuir*, 2011, **27**, 6295; (*b*) D. A. Ruddy and T. D. Tilley, *J. Am. Chem. Soc.*, 2008, **130**, 11088.
27 (*a*) A. Bodor, I. Bányai and I. Tóth, *Coord. Chem. Rev.*, 2002, **228**, 175; (*b*) L. L. Justino, M. L. Ramos, M. M. Caldeira and V. M. Gil, *Inorg. Chim. Acta*, 2000, **311**, 119.
28 (*a*) D. Bayot, B. Tinant and M. Devillers, *Inorg. Chim. Acta*, 2004, **357**, 809; (*b*) C. Djordjevic, N. Vuletic, B. A. Jacobs, M. Lee-Renslo and E. Sinn, *Inorg. Chem.*, 1997, **36**, 1798; (*c*) D. Bayot, B. Tinant and M. Devillers, *Inorg. Chem.*, 2004, **43**, 5999; (*d*) A. Maniatakou, C. Makedonas, C. A. Mitsopoulou, C. Raptopoulou, I. Rizopoulou, A. Terzis and A. Karaliota, *Polyhedron*, 2008, **27**, 3398.
29 (*a*) G. Aygun and R. Turan, *Thin Solid Films*, 2008, **517**, 994; (*b*) J. Capilla, J. Olivares, M. Clement, J. Sangrador, E. Iborra and A. Devos, presented in part at 2011 Joint Conference of the IEEE International Frequency Control and the European Frequency and Time Forum (FCS) Proceedings, IEEE service centre, 2011; (*c*) A. Fielicke, G. Meijer and G. Von Helden, *Eur. Phys. J. D*, 2003, **24**, 69.
30 I. C. McNeill and S. M. T. Sadeghi, *Polym. Degrad. Stab.*, 1990, **30**, 213.
31 D. D. Jiang, Q. Yao, M. A. McKinney and C. A. Wilkie, *Polym. Degrad. Stab.*, 1999, **63**, 423.
32 A. Periasamy, S. Muruganand and M. Palaniswamy, *Rasayan J. Chem.*, 2009, **2**, 981.
33 (*a*) A. C. Dengel and W. P. Griffith, *Polyhedron*, 1989, **8**, 1371; (*b*) V. Petrykin, M. Kakihana, K. Yoshioka, S. Sasaki, Y. Ueda, K. Tomita, Y. Nakamura, M. Shiro and A. Kudo, *Inorg. Chem.*, 2006, **45**, 9251; (*c*) D. Bayot, B. Tinant and M. Devillers, *Inorg. Chem.*, 2005, **44**, 1554.
34 S. R. Gogoi, K. Ahmed, G. Saikia and N. S. Islam, *J. Indian Chem. Soc.*, 2018, **95**, 801.
35 (*a*) B. Delley, *J. Chem. Phys.*, 1990, **92**, 508; (*b*) J. P. Perdew and Y. Wang, *Phys. Rev. B: Condens. Matter Mater. Phys.*, 1992, **45**, 13244. Calculations were done using density functional theory (DFT).
36 (*a*) L. C. Passoni, M. R. H. Siddiqui, A. Steiner and I. V. Kozhevnikov, *J. Mol. Catal. A: Chem.*, 2000, **153**, 103; (*b*) D. Bayot, B. Tinant, B. Mathieu, J. P. Declercq and M. Devillers, *Eur. J. Inorg. Chem.*, 2003, 737; (*c*) A. Maniatakou, C. Makedonas, C. A. Mitsopoulou, C. Raptopoulou, I. Rizopoulou, A. Terzis and A. Karaliota, *Polyhedron*, 2008, **27**, 3398.
37 (*a*) S. Bhattacharjee, *Curr. Sci.*, 2005, 1113; (*b*) G. W. Winston, *Stress Responses in Plants: Adaptation and Acclimation Mechanisms*, Willy-Liss Inc., New York, 1990, pp. 57–86; (*c*) C. H. Foyer, in *Molecular Biology of Free Radical Scavenging Enzymes*, ed. J. Scandalios, Cold Spring Harbor Laboratory, New York, 1997.
38 (*a*) T. Ramasarma, in *Vanadium Biochemistry*, ed. M. A. Alves, Research Signpost, India, 2007, pp. 45–76; (*b*) T. Ramasarma, *Proc. Indian Natl. Sci. Acad.*, 2003, **69**, 649; (*c*) N. Chatterjee, S. Kiran, B. M. Ram, N. Islam, T. Ramasarma and G. Ramakrishna, *Mech. Ageing Dev.*, 2011, **132**, 230; (*d*) M. Giorgio, M. Trinei, E. Migliaccio and P. G. Pelicci, *Nat. Rev. Mol. Cell Biol.*, 2007, **8**, 722; (*e*) B. J. Goldstein, K. Mahadev and X. Wu, *Diabetes*, 2005, **54**, 311; (*f*) B. Chance, H. Sies and A. Boveris, *Physiol. Rev.*, 1979, **59**, 527.
39 H. N. Ravishankar, A. V. Rao and T. Ramasarma, *Arch. Biochem. Biophys.*, 1995, **321**, 477.
40 (*a*) P. Hazarika, D. Kalita and N. S. Islam, *J. Enzyme Inhib. Med. Chem.*, 2008, **23**, 504; (*b*) D. Kalita, S. P. Das and N. S. Islam, *Biol. Trace Elem. Res.*, 2009, **128**, 200; (*c*) P. Hazarika, D. Kalita and S. Sarmah, *Mol. Cell. Biochem.*, 2006, **284**, 39.
41 P. Hazarika, S. Sarmah, D. Kalita and N. S. Islam, *Transition Met. Chem.*, 2008, **33**, 69.
42 (*a*) R. Albrecht, J. Le Petit, V. Calvert, G. Terrom and C. Périssol, *Bioresour. Technol.*, 2010, **101**, 228; (*b*) H. U. Bergmeyer, J. Bergmeyer and M. Grassl, *Methods of Enzymatic Analysis*, VerlagChemie, Weinheim, 1983.
43 (*a*) H. Lineweaver and D. Burk, *J. Am. Chem. Soc.*, 1934, **56**, 658; (*b*) A. Cornish-Bowden, *Perspect. Sci.*, 2014, **1**, 74.
44 (*a*) P. J. Stankiewicz and M. J. Gresser, *Biochemistry*, 1988, **27**, 206; (*b*) Y. S. Heo, J. M. Ryu, S. M. Park, J. H. Park, H. C. Lee, K. Y. Hwang and J. S. Kim, *Exp. Mol. Med.*, 2002, **34**, 211; (*c*) R. L. VanEtten, P. P. Waymack and D. M. Rehkop, *J. Am. Chem. Soc.*, 1974, **96**, 6782; (*d*) G. Soman, Y. C. Chang and D. J. Graves, *Biochemistry*, 1983, **22**, 4994.
45 D. K. Lord, N. C. Cross, M. A. Bevilacqua, S. H. Rider, P. A. Gorman, A. V. Groves, D. W. Moss, D. Sheer and T. M. Cox, *FEBS J.*, 1990, **189**, 287.
46 J. B. Vincent, M. W. Crowder and B. A. Averill, *Biochemistry*, 1991, **30**, 3025.
47 (*a*) H. Bull, P. G. Murray, D. Thomas, A. M. Fraser and P. N. Nelson, *Mol. Pathol.*, 2002, **55**, 65; (*b*) D. F. Hunt, J. R. Yates, J. Shabanowitz, N. Z. Zhu, T. Zirino, B. A. Averill, S. T. Daurat-Larroque, J. G. Shewale, R. M. Roberts and K. Brew, *Biochem. Biophys. Res. Commun.*, 1987, **144**, 1154; (*c*) C. M. Ketcham, R. M. Roberts, R. C. Simmen and H. S. Nick, *J. Biol. Chem.*, 1989, **264**, 557.

48 D. C. Crans, in *Vanadium compounds: Chemistry, biochemistry, and therapeutic applications*, ed. A. S. Tracey and D. C. Crans, Oxford University Press, UK, 1998, pp. 82–103.
49 G. Saikia, PhD thesis, Tezpur University, 2020.
50 S. Sarmah, P. Hazarika and N. S. Islam, *Mol. Cell. Biochem.*, 2002, **236**, 95.
51 M. K. Chaudhuri, S. K. Ghosh and N. S. Islam, *Inorg. Chem.*, 1985, **24**, 2706.
52 G. Saikia, K. Ahmed, C. Rajkhowa, M. Sharma, H. Talukdar and N. S. Islam, *New J. Chem.*, 2019, **43**, 17251.
53 C. V. Ferreira, E. M. Taga and H. Aoyama, *Plant Sci.*, 1999, **147**, 49.

